Chemical Science

ROYAL SOCIETY OF CHEMISTRY

EDGE ARTICLE

View Article Online
View Journal | View Issue

Cite this: *Chem. Sci.*, 2026, **17**, 1778

All publication charges for this article have been paid for by the Royal Society of Chemistry

Supramolecular host–guest modulated thermally activated delayed fluorescence for photodynamic therapy

Xujun Qiu, Peiqi Hu, Angelica Sevilla-Pym, Jana R. Caine and Zachary M. Hudson *

Received 9th October 2025
Accepted 25th November 2025

DOI: 10.1039/d5sc07827j

rsc.li/chemical-science

Supramolecular host–guest chemistry can tune the photophysical behavior of organic emitters by confining them within well-defined nanoscale environments. Here we report a straightforward strategy to modulate the thermally activated delayed fluorescence (TADF) properties of organic emitters in aqueous media through complexation with the macrocyclic host cucurbit[7]uril (CB[7]). Upon formation of the TADF-CB[7] complex, the photoluminescence quantum yield is enhanced due to the suppression of non-radiative decay pathways within the rigid host cavity. Furthermore, host–guest encapsulation was found to accelerate both forward and reverse intersystem crossing, resulting in improved access to the triplet state. In the presence of molecular oxygen, this facilitates an increased generation of cytotoxic singlet oxygen, thereby boosting the efficacy of photodynamic therapy (PDT). These findings provide a promising supramolecular approach to advancing the application of TADF materials in aqueous-phase PDT systems.

Introduction

Photodynamic therapy (PDT) has emerged as a promising cancer treatment modality since its first clinical approval in 1993.[1] Compared with conventional clinical approaches including chemotherapy, radiotherapy and surgery, PDT is less invasive and offers spatiotemporal specificity, low systemic toxicity, and minimal drug resistance.[2,3] In this light-driven process, photosensitizers (PSs) are first excited by photons from the ground state to the lowest singlet excited state (S_1), followed by population of the lowest triplet excited state (T_1) *via* intersystem crossing (ISC). The T_1 state then interacts with the surrounding ground state oxygen ($^3O_2$) to generate cytotoxic reactive oxygen species (ROS), such as singlet oxygen ($^1O_2$), leading to irreversible cellular damage in the targeted region.[4,5] The efficient generation of long-lived triplet states is thus essential for PDT.

Thermally activated delayed fluorescence (TADF) materials have recently attracted significant attention as prospective candidates for PDT, owing to their long-lived triplet states, high photoluminescence efficiency, and tunable photophysical properties.[6,7] Due to the minimal overlap between the highest occupied molecular orbital (HOMO) and the lowest unoccupied molecular orbital (LUMO), TADF emitters typically exhibit a small singlet–triplet energy gap (ΔE_{ST}, generally $\leq$ 0.2 eV). This facilitates efficient reverse ISC (rISC) from T_1 to S_1, driven by ambient thermal energy, resulting in delayed fluorescence.[8–11] Meanwhile, the narrow ΔE_{ST} also promotes efficient ISC, which facilitates triplet generation and enhances interaction with oxygen molecules, thereby boosting ROS production. Accordingly, TADF materials have recently emerged as efficient PSs for PDT.[12–15]

However, the inherent hydrophobicity of most TADF emitters limits their applicability in biological systems. To introduce them into aqueous media, various strategies inspired by nanomaterials have been employed, including the self-assembly of TADF molecules into nanoaggregates,[12,16–18] encapsulation with amphiphilic surfactants,[19–21] and incorporation into polymer dots.[22–26] Despite their utility, these approaches often suffer from aggregation-caused quenching, dye leakage, and limited oxygen permeability. To address these issues, our group has developed nanoparticles from amphiphilic block copolymers incorporating both a TADF imaging probe and a distinct BODIPY PS to yield a theranostic platform for image-guided PDT.[27] This approach, however, is synthetically complex, and requires a secondary dye to act as the PS. A simpler approach that enables the direct use of the TADF material for PDT in water would thus be highly desirable.

Supramolecular systems based on hydrophilic macrocyclic hosts, such as cucurbiturils and cyclodextrins, provide one such option for encapsulating hydrophobic dyes in water.[28,29] The supramolecular host–guest interaction can suppress non-radiative decay by restricting molecular motion, while also minimizing the quenching of triplets by isolating the dye from

Department of Chemistry, The University of British Columbia, 2036 Main Mall, Vancouver, British Columbia, V6T 1Z1, Canada. E-mail: zhudson@chem.ubc.ca; Fax: +1-604-822-2847; Tel: +1-604-822-3266

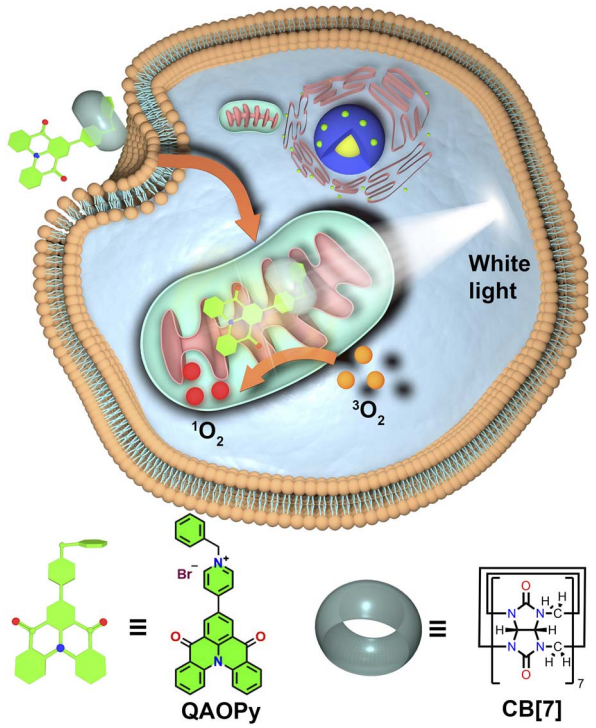

Scheme 1 Schematic illustration of supramolecular host CB[7] modulated TADF for mitochondria-targeted photodynamic therapy.

the surrounding medium.[30–35] These features lay the foundation for productive $^1O_2$ generation in PDT.[36–42]

Among the various types of TADF materials, multi-resonance TADF (MR-TADF) compounds stand out for their exceptional photophysical properties. Owing to their rigid molecular structures and localized excited states, MR-TADF materials feature narrow emission bands, high photoluminescence quantum yields (Φ_{PL}), and improved photostability.[43–47] This unique combination of photophysical properties make MR-TADF emitters highly attractive for biological applications, particularly in high-resolution bioimaging.[48,49]

Herein, we describe a water-soluble MR-TADF material **QAOPy** and its host–guest complexation with curcurbit[7]uril (CB[7]) in water (Scheme 1). Upon complexation with (CB[7]) in a 1 : 1 molar ratio, the resulting **QAOPy-CB[7]** host–guest complex exhibited a significantly enhanced Φ_{PL} of 52.1% in degassed water, compared to 36.1% for the unbound **QAOPy**. Both **QAOPy** and its CB[7] complex displayed clear delayed fluorescence in degassed water, with lifetimes (τ_d) of 59.4 μs and 45.1 μs, respectively. We also demonstrate how encapsulation in CB[7] leads to improved $^1O_2$ generation and therapeutic efficiency relative to the unbound **QAOPy** molecule. To the best of our knowledge, this is the first demonstration of PDT using supramolecular host–guest TADF materials.

Results and discussion

Synthesis and host–guest study

The synthesis and characterization of **QAOPy** are detailed in the SI (Fig. S1–S4). Owing to the presence of a pyridinium group, **QAOPy** is water soluble, and can act as a suitable guest for complexation with CB[7].[50] The host–guest interaction was first investigated using proton nuclear magnetic resonance (^{1}H NMR) spectroscopy. As shown in Fig. 1a, S5 and S6, the addition of an equimolar amount of CB[7] to **QAOPy** caused notable upfield shifts in the proton signals associated with the benzyl moiety (H_1–H_4) and the pyridinium group (H_5), suggesting deep encapsulation within the CB[7] cavity. Meanwhile, protons H_6–H_{11} exhibited downfield shifts, indicating their positioning near the portal region of the macrocycle.[51,52]

Next, the formation of the 1 : 1 **QAOPy-CB[7]** complex was further confirmed by electrospray ionization mass spectrometry (ESI-MS). A peak with a mass-to-charge ratio (m/z) of 1627.5022 was found, corresponding to the intact **QAOPy-CB[7]** complex (Fig. 1b and S7). To quantify the binding affinity between **QAOPy** and CB[7], UV-vis titration was performed. As CB[7] was gradually added to a **QAOPy** solution, a continuous decrease in absorbance at 400 nm was observed, along with the emergence of isosbestic points (Fig. 1c), indicating a clean conversion between the free and complexed states. The absorbance changes were fitted to a direct binding assay model,[53] yielding a binding constant of $(2.71 \pm 0.06) \times 10^6$ M^{-1} (Fig. S8).

Photophysical characterization

The photophysical properties of **QAOPy** and its supramolecular complex **QAOPy-CB[7]** were investigated in Milli-Q water. As depicted in Fig. 1c, both compounds feature two main absorption peaks below 400 nm and an additional peak beyond 450 nm, corresponding to locally excited (LE) π–π* and short-range charge transfer transitions, respectively.[54] In the aerated state (Fig. 2a and Table S1), **QAOPy** displays green fluorescence with an emission maximum (λ_{em}) at 509 nm, a full width at half maximum (FWHM) of 67 nm, and an absolute Φ_{PL} of 32.2%. Upon complexation with CB[7], **QAOPy-CB[7]** exhibits a slightly red-shifted λ_{em} at 509 nm, a narrower FWHM of 65 nm, and a significantly enhanced Φ_{PL} of 38.9%. Under nitrogen atmosphere, **QAOPy** shows a modest redshift to 512 nm with an unchanged FWHM and an increased Φ_{PL} of 36.1%, while **QAOPy-CB[7]** maintains its emission maximum at 506 nm with a FWHM of 63 nm and a further enhanced Φ_{PL} of 52.1%. The encapsulation within the CB[7] cavity partially restricts intramolecular rotations, thereby suppressing non-radiative decay pathways and enhancing Φ_{PL}.

Time-resolved photoluminescence measurements revealed that the prompt fluorescence lifetimes (τ_p) of **QAOPy** were 8.20 ns in air and 8.51 ns under nitrogen atmosphere. Similarly, the **QAOPy-CB[7]** complex exhibited prompt lifetimes of 8.71 ns and 8.73 ns in air and nitrogen, respectively (Fig. S9). In contrast, delayed fluorescence lifetimes (τ_d) measured in degassed water showed a τ_d of 59.4 μs for **QAOPy** and 45.1 μs for **QAOPy-CB[7]**, while under aerated conditions, the lifetimes shortened to 4.14 μs and 6.20 μs, respectively (Fig. 2b and S10), reflecting the quenching effect of molecular oxygen on triplet states. The optical bandgaps of both **QAOPy** and **QAOPy-CB[7]** were determined to be 2.64 eV (Fig. S11).

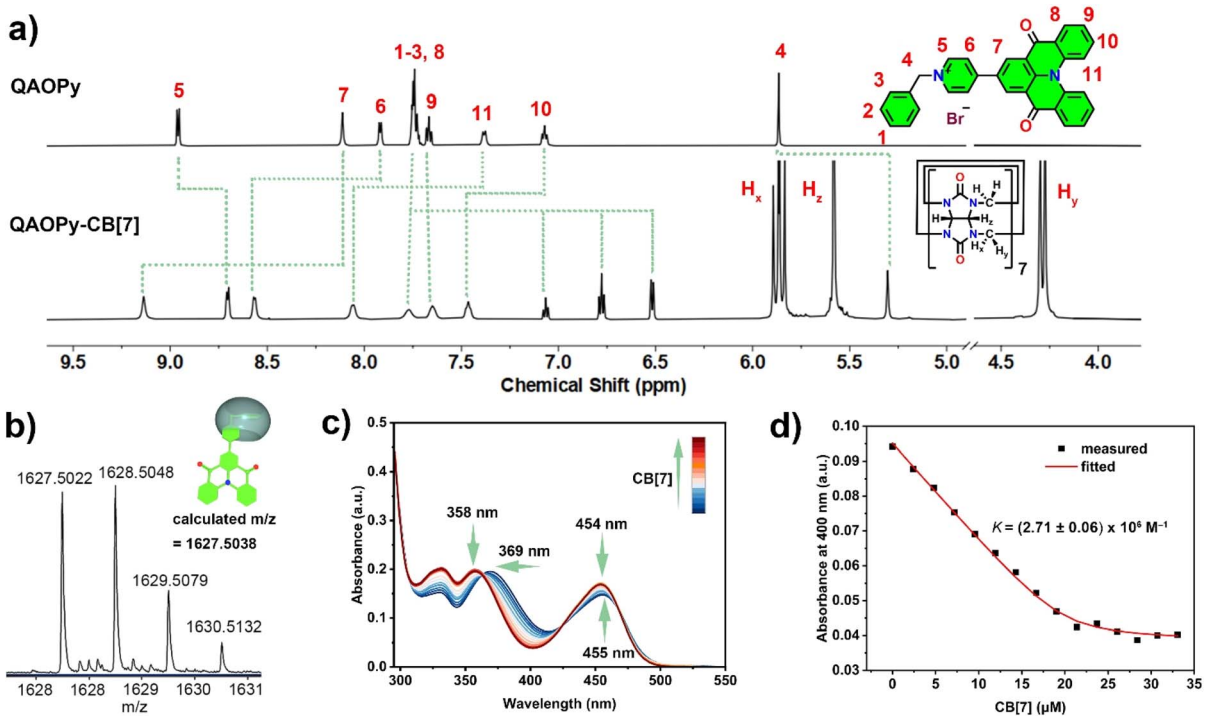

Fig. 1 (a) ^{1}H NMR (600 MHz, D_2O, 298 K) spectra of **QAOPy** (0.5 mM) and the **QAOPy-CB[7]** host–guest complex (1 : 1, 0.5 mM), showing characteristic chemical shift changes upon complexation. D_2O peaks were omitted for clarity; (b) ESI-MS spectrum of **QAOPy-CB[7]**; (c) UV-vis absorption spectra of **QAOPy** (20 μM) upon titration with increasing concentrations of CB[7] (0–33.0 μM) in aqueous solution at 298 K; (d) nonlinear least-squares fitting of the absorbance changes at 400 nm against the concentration of CB[7] for determining the binding constant between **QAOPy** and CB[7].

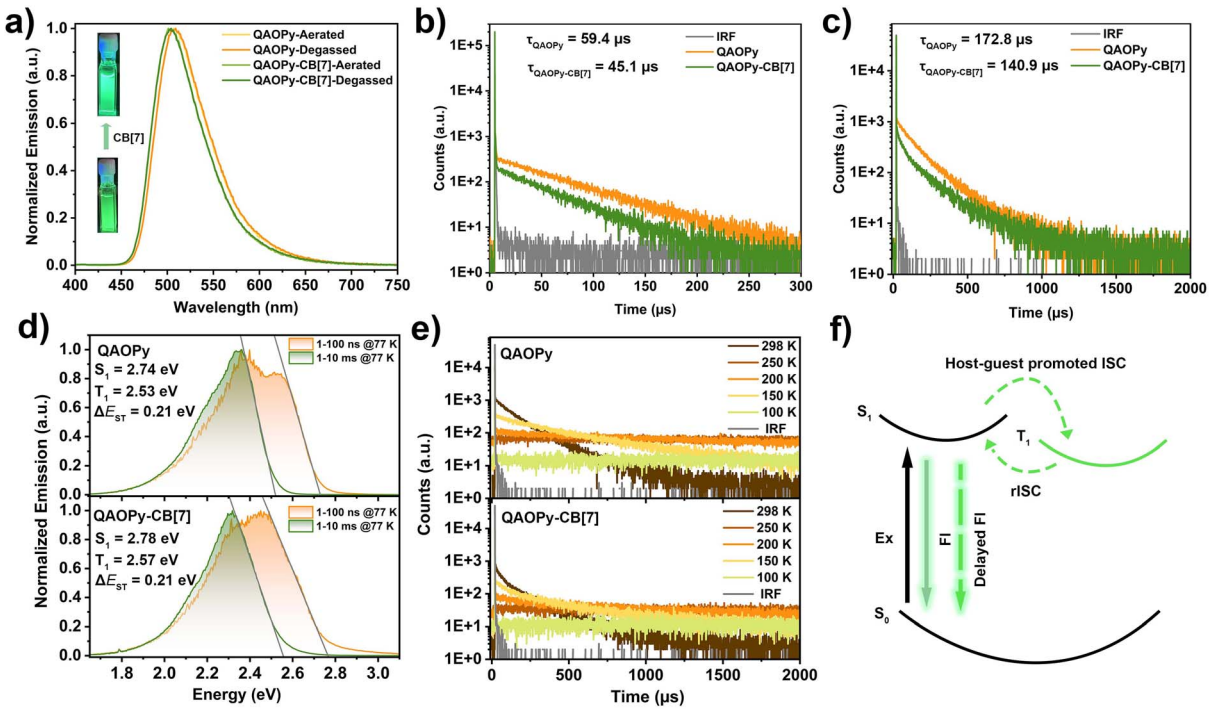

Fig. 2 (a) PL spectra of **QAOPy** (10 μM) and the **QAOPy-CB[7]** host–guest complex (1 : 1, 10 μM) in aerated and degassed Milli-Q water. Inset: photographs of **QAOPy** and **QAOPy-CB[7]** under UV illumination (365 nm); (b) time-resolved PL decay profiles of **QAOPy** (10 μM) and **QAOPy-CB[7]** (1 : 1, 10 μM) in degassed Milli-Q water (λ_{exc} = 375 nm); (c) time-resolved PL decay spectra of **QAOPy** and **QAOPy-CB[7]** in 1 wt% HA film at 298 K (λ_{exc} = 375 nm); (d) prompt and phosphorescence emission spectra of **QAOPy** and **QAOPy-CB[7]** in 1 wt% HA film at 77 K (λ_{exc} = 375 nm), recorded over 1–100 ns and 1–10 ms time windows, respectively; (e) temperature-dependent time-resolved PL decay profiles of **QAOPy** and **QAOPy-CB[7]** in 1 wt% HA film (λ_{exc} = 375 nm); (f) schematic illustration of host–guest complexation-enhanced ISC facilitated by CB[7] encapsulation.

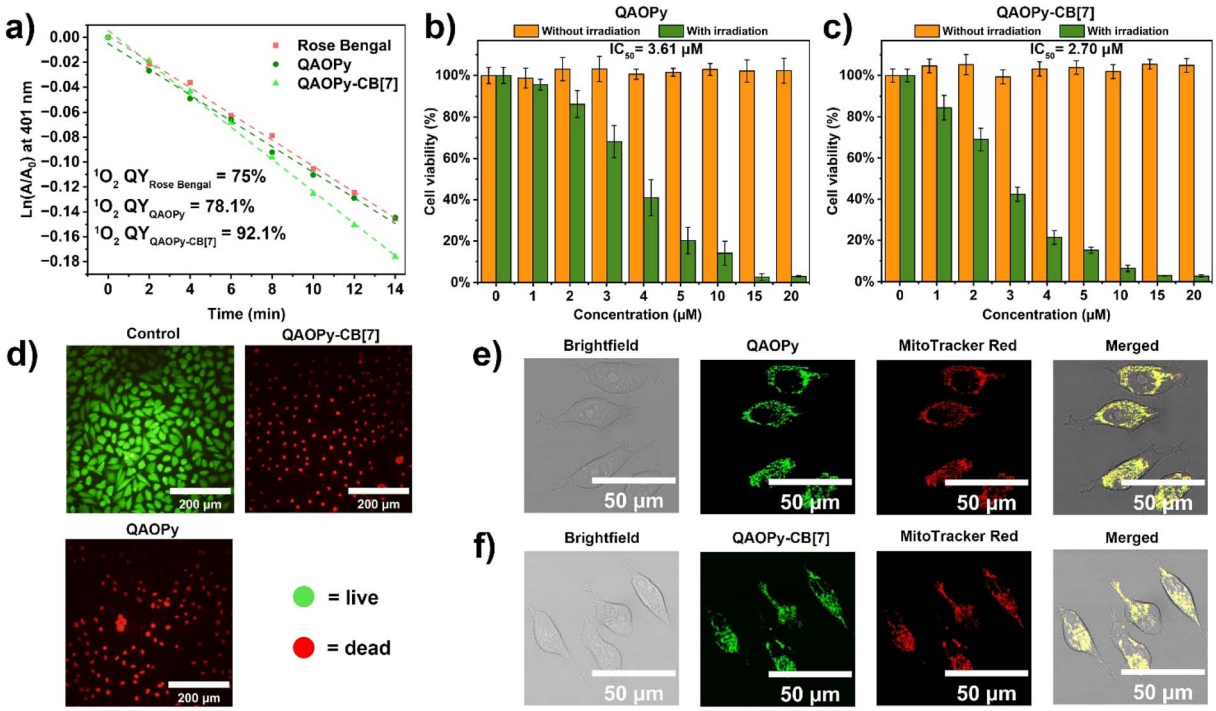

Fig. 3 (a) Photodynamic activity assessed *via* ABMM degradation assay: decomposition rate constants of ABMM (λ_{max} = 401 nm) in the presence of Rose Bengal, **QAOPy** and **QAOPy-CB[7]**; cell viability assays of HeLa cells treated with varying concentrations of (b) **QAOPy** and (c) **QAOPy-CB[7]** for 24 h, measured under darkness and white light conditions (30 min irradiation after 2 hour incubation); (d) confocal laser scanning microscopy images of live/dead staining of HeLa cells treated with **QAOPy** and **QAOPy-CB[7]** for 2 h and followed by 30 min white light irradiation, using FDA (green, live cells) and PI (red, dead cells); confocal live cell images of Hela cell incubated with (e) **QAOPy** and (f) **QAOPy-CB[7]** (1 μM) for 2 h, followed by MitoTracker Red CMXRos for 30 min (λ_{exc} = 448 nm for **QAOPy** and **QAOPy-CB[7]**, and 561 nm for MitoTracker Red, respectively).

To further investigate the solid-state photophysical behavior of **QAOPy** and its host–guest complex **QAOPy-CB[7]**, hyaluronic acid (HA) was employed as an inert matrix to fabricate thin films. A doping concentration of 1 wt% was chosen to avoid aggregation-caused quenching,[55] which can occur at higher concentrations of **QAOPy**. Time-resolved PL decay profiles of the films revealed multiexponential decay kinetics. At room temperature, the τ_p were measured as 6.74 ns for **QAOPy** and 6.59 ns for **QAOPy-CB[7]**. The delayed lifetime τ_d were found to be 172.8 μs for **QAOPy** and 140.9 μs for **QAOPy-CB[7]**, with Φ_{PL} of 17.6% and 36.5%, respectively (Fig. 2c and S12). These trends are consistent with those observed in aqueous solution.

The singlet (S_1) and triplet (T_1) energy levels were estimated from the onset of the prompt fluorescence and phosphorescence spectra collected at 77 K, revealing a small ΔE_{ST} of 0.21 eV for both systems (Fig. 2d). Furthermore, temperature-dependent time-resolved PL measurements showed an increase in delayed emission intensity with rising temperature, a hallmark feature of TADF (Fig. 2e). The intersystem crossing rate constant (k_{ISC}) and reverse intersystem crossing rate constant (k_{rISC}) were determined to be 1.32×10^7 s^{-1} and 1.89×10^4 s^{-1} for **QAOPy**, respectively. For **QAOPy-CB[7]**, the corresponding values were calculated as 2.91×10^7 s^{-1} for k_{ISC} and 2.97×10^4 s^{-1} for k_{rISC} (Table S1). These findings indicate that the presence of CB[7] enhances the ISC and rISC processes (Fig. 2f). Since both the rate of ISC and the ISC/rISC ratio[56] are higher for the supramolecular complex, it should provide a higher concentration of triplets under irradiation than the uncomplexed TADF molecule. Encapsulation of the TADF dye (**QAOPy**) within the CB[7] cavity significantly modifies its excited-state dynamics even though the ΔE_{ST} remains unchanged. The confined environment rigidifies the molecular framework and reduces nonradiative decay pathways, thereby increasing the population available for ISC. In addition, the electrostatically rich carbonyl portals of CB[7] stabilize the charge-transfer character of the excited states, enhancing spin–vibronic coupling and promoting both ISC and subsequent rISC. These effects collectively increase the utilization efficiency of triplet excitons.

Photodynamic therapy and cellular imaging

Encouraged by these promising photophysical properties, we evaluated the $^1O_2$ generation efficiency of **QAOPy** and **QAOPy-CB[7]**, using Rose Bengal (RB), a well-established photosensitizer with a $^1O_2$ quantum yield ($^1O_2$ QY) of 75% in H_2O, as a ref. 57. The singlet oxygen probe α,α′-(anthracene-9,10-diyl) bis(methylmalonate) (ABMM) was employed, which reacts rapidly and specifically with $^1O_2$. Upon light irradiation, the characteristic absorption peak of the anthracene moiety in ABMM at 401 nm gradually decreased (Fig. S14), allowing quantification of $^1O_2$ production by monitoring its decomposition kinetics. Using this approach, the $^1O_2$ QY for **QAOPy** and

QAOPy-CB[7] were determined to be 78.1% and 92.1%, respectively (Fig. 3a, S15 and S16).

These results support our hypothesis that host–guest encapsulation with CB[7] facilitates ISC, thereby enhancing the generation of triplet states and boosting $^1O_2$ generation (Fig. 2f), which is a desirable trait for PDT. Moreover, photostability tests showed that both **QAOPy** and **QAOPy-CB[7]** exhibit good stability for up to 60 min of continuous irradiation with a 4.55 mW Xe lamp, (Fig. S17), with the latter benefiting from improved stability due to the protective effect of CB[7]'s confined cavity.

Given the efficient $^1O_2$ generation observed for **QAOPy** and **QAOPy-CB[7]**, their photodynamic therapeutic potential was further assessed *in vitro* using HeLa cells. As shown in Fig. 3b and c, both compounds exhibited negligible cytotoxicity under dark conditions, confirming their biocompatibility in the absence of light. Upon white light irradiation, however, significant phototoxicity was observed, with IC_{50} of 3.61 μM for **QAOPy** and 2.70 μM for **QAOPy-CB[7]**, respectively, which indicates enhanced PDT efficacy upon host–guest encapsulation.

Fluorescence-based live/dead cell assays using fluorescein diacetate (FDA) and propidium iodide (PI) further corroborated these results (Fig. 3d). FDA stains live cells *via* esterase-mediated hydrolysis to green-fluorescent fluorescein, while PI labels dead cells by intercalating with nuclear DNA.[58] Confocal microscopy imaging revealed strong colocalization of both **QAOPy** and **QAOPy-CB[7]** with MitoTracker Red, indicating a clear preference for mitochondrial accumulation. This was further supported by high Pearson's correlation coefficients of 0.893 for **QAOPy** and 0.890 for **QAOPy-CB[7]**, confirming their efficient mitochondrial targeting capabilities (Fig. 3e and f). This subcellular targeting likely contributes to the elevated photodynamic therapeutic efficiency observed.[16]

Conclusions

In summary, we report a supramolecular strategy for the use of TADF compounds in aqueous media by encapsulation with CB[7]. Host–guest complexation enhances ISC and rISC, improving access to the triplet state of the TADF material. As a result, the TADF-CB[7] system exhibits a higher $^1O_2$ QY and improved photodynamic therapeutic efficiency compared to the uncomplexed molecule. This approach provides a new strategy for designing high-performance TADF-based photosensitizers for theranostic and biomedical applications, particularly in PDT, as well as a method for tuning the photophysical properties of TADF materials *via* supramolecular chemistry.

Author contributions

X. Q.: conceptualization (lead); formal analysis (lead); investigation (lead); methodology (lead); visualization (lead); writing – original draft preparation (lead); writing – review and editing (equal). P. H.: resources (supporting); writing – original draft preparation (supporting); writing – review and editing (supporting). A. S.-P.: investigation (supporting); formal analysis (supporting); writing – review and editing (supporting). J. R. C.: methodology (supporting); validation (supporting). Z. M. H.: funding acquisition (lead); project administration (lead); supervision (lead); validation (supporting); writing – review and editing (equal).

Conflicts of interest

The authors declare no conflict of interest.

Data availability

The data supporting this article have been included as part of the supplementary information (SI). Supplementary information: additional synthetic schemes, general experimental considerations, and additional characterization data related to photophysical, cell culture. See DOI: https://doi.org/10.1039/d5sc07827j.

Acknowledgements

The authors thank the Natural Sciences and Engineering Research Council of Canada (NSERC), the Canada Foundation for Innovation (CFI), and the British Columbia Knowledge Development Fund (BCKDF) for financial support. P. H. thanks UBC for a Four-Year Doctoral Fellowship, and A. S.-P. thanks UBC for an Agnes and Gilbert Hooley Scholarship. J. R. C. thanks NSERC for a Canada Graduate Research Scholarship. Z. M. H. is grateful for a Killam Research Accelerator Fellowship and a Canada Research Chair. The authors gratefully acknowledge support from the UBC Chemistry Biological Services Laboratory and the Life Sciences Institute Imaging Core Facility (RRID:SCR_023783) during this project. The authors would also like to thank Dr Saeid Kamal for helpful discussions, and to Pengfei Xu for assistance with NMR measurements.

Notes and references

1 Z. Huang, *Technol. Cancer Res. Treat.*, 2005, **4**, 283–293.
2 G. Obaid, J. P. Celli, M. Broekgaarden, A.-L. Bulin, P. Uusimaa, B. Pogue, T. Hasan and H.-C. Huang, *Nat. Rev. Bioeng.*, 2024, **2**, 752–769.
3 S. S. Lucky, K. C. Soo and Y. Zhang, *Chem. Rev.*, 2015, **115**, 1990–2042.
4 J. P. Celli, B. Q. Spring, I. Rizvi, C. L. Evans, K. S. Samkoe, S. Verma, B. W. Pogue and T. Hasan, *Chem. Rev.*, 2010, **110**, 2795–2838.
5 S. Kwiatkowski, B. Knap, D. Przystupski, J. Saczko, E. Kędzierska, K. Knap-Czop, J. Kotlińska, O. Michel, K. Kotowski and J. Kulbacka, *Biomed. Pharmacother.*, 2018, **106**, 1098–1107.
6 F. Fang, L. Zhu, M. Li, Y. Song, M. Sun, D. Zhao and J. Zhang, *Adv. Sci.*, 2021, **8**, 2102970.
7 Z. Li, J. Lu and X. Li, *Chem. Eur J.*, 2024, **30**, e202401001.
8 H. Uoyama, K. Goushi, K. Shizu, H. Nomura and C. Adachi, *Nature*, 2012, **492**, 234–238.
9 Y. Tao, K. Yuan, T. Chen, P. Xu, H. Li, R. Chen, C. Zheng, L. Zhang and W. Huang, *Adv. Mater.*, 2014, **26**, 7931–7958.

10 M. Y. Wong and E. Zysman-Colman, *Adv. Mater.*, 2017, **29**, 1605444.
11 J. M. Dos Santos, D. Hall, B. Basumatary, M. Bryden, D. Chen, P. Choudhary, T. Comerford, E. Crovini, A. Danos, J. De, S. Diesing, M. Fatahi, M. Griffin, A. K. Gupta, H. Hafeez, L. Hämmerling, E. Hanover, J. Haug, T. Heil, D. Karthik, S. Kumar, O. Lee, H. Li, F. Lucas, C. F. R. Mackenzie, A. Mariko, T. Matulaitis, F. Millward, Y. Olivier, Q. Qi, I. D. W. Samuel, N. Sharma, C. Si, L. Spierling, P. Sudhakar, D. Sun, E. Tankelevičiūtė, M. Duarte Tonet, J. Wang, T. Wang, S. Wu, Y. Xu, L. Zhang and E. Zysman-Colman, *Chem. Rev.*, 2024, **124**, 13736–14110.
12 J. Zhang, W. Chen, R. Chen, X.-K. Liu, Y. Xiong, S. V. Kershaw, A. L. Rogach, C. Adachi, X. Zhang and C.-S. Lee, *Chem. Commun.*, 2016, **52**, 11744–11747.
13 F. Fang, Y. Yuan, Y. Wan, J. Li, Y. Song, W.-C. Chen, D. Zhao, Y. Chi, M. Li, C.-S. Lee and J. Zhang, *Small*, 2022, **18**, 2106215.
14 W. Chen, Z. Wang, M. Tian, G. Hong, Y. Wu, M. Sui, M. Chen, J. An, F. Song and X. Peng, *J. Am. Chem. Soc.*, 2023, **145**, 8130–8140.
15 J. Zhang, J. Ma, S. Zhang, X. Lou, Y. Ding, Y. Li, M. Xu, X. Xie, X. Jiao, X. Dou, X. Wang and B. Tang, *ACS Nano*, 2023, **17**, 23430–23441.
16 J. Zhang, F. Fang, B. Liu, J.-H. Tan, W.-C. Chen, Z. Zhu, Y. Yuan, Y. Wan, X. Cui, S. Li, Q.-X. Tong, J. Zhao, X.-M. Meng and C.-S. Lee, *ACS Appl. Mater. Interfaces*, 2019, **11**, 41051–41061.
17 S. Hu, B. Huang, Y. Pu, C. Xia, Q. Zhang, S. Guo, Y. Wang and X. Huang, *J. Mater. Chem. B*, 2021, **9**, 5645–5655.
18 D. Barman, P. Rajamalli, A. P. Bidkar, T. Sarmah, S. S. Ghosh, E. Zysman-Colman and P. K. Iyer, *Small*, 2025, **21**, 2409533.
19 Y.-F. Xiao, J.-X. Chen, S. Li, W.-W. Tao, S. Tian, K. Wang, X. Cui, Z. Huang, X.-H. Zhang and C.-S. Lee, *Chem. Sci.*, 2020, **11**, 888–895.
20 Y.-F. Xiao, J.-X. Chen, W.-C. Chen, X. Zheng, C. Cao, J. Tan, X. Cui, Z. Yuan, S. Ji, G. Lu, W. Liu, P. Wang, S. Li and C.-S. Lee, *Chem. Commun.*, 2021, **57**, 4902–4905.
21 J. R. Caine, P. Hu, A. T. Gogoulis and Z. M. Hudson, *Acc. Mater. Res.*, 2023, **4**, 879–891.
22 C. J. Christopherson, N. R. Paisley, Z. Xiao, W. R. Algar and Z. M. Hudson, *J. Am. Chem. Soc.*, 2021, **143**, 13342–13349.
23 N. R. Paisley, S. V. Halldorson, M. V. Tran, R. Gupta, S. Kamal, W. R. Algar and Z. M. Hudson, *Angew. Chem., Int. Ed.*, 2021, **60**, 18630–18638.
24 K.-F. Hsu, S.-P. Su, H.-F. Lu, M.-H. Liu, Y. J. Chang, Y.-J. Lee, H. K. Chiang, C.-P. Hsu, C.-W. Lu and Y.-H. Chan, *Chem. Sci.*, 2022, **13**, 10074–10081.
25 Y. Luo, B. Zhao, B. Zhang, Y. Lan, L. Chen, Y. Zhang, Y. Bao and L. Niu, *Analyst*, 2022, **147**, 2442–2451.
26 A. Sevilla-Pym, W. L. Primrose, B. T. Luppi, K. Bergmann and Z. M. Hudson, *ACS Appl. Mater. Interfaces*, 2024, **16**, 46133–46144.
27 B. T. Luppi, W. L. Primrose and Z. M. Hudson, *Angew. Chem., Int. Ed.*, 2024, **63**, e202400712.
28 G. Crini, *Chem. Rev.*, 2014, **114**, 10940–10975.
29 K. I. Assaf and W. M. Nau, *Chem. Soc. Rev.*, 2015, **44**, 394–418.
30 D. Li, F. Lu, J. Wang, W. Hu, X.-M. Cao, X. Ma and H. Tian, *J. Am. Chem. Soc.*, 2018, **140**, 1916–1923.
31 D. Li, Z. Liu, M. Fang, J. Yang, B. Z. Tang and Z. Li, *ACS Nano*, 2023, **17**, 12895–12902.
32 Z.-Y. Zhang, Y. Chen and Y. Liu, *Angew. Chem., Int. Ed.*, 2019, **58**, 6028–6032.
33 X. Qiu, Y. Wang, S. Leopold, S. Lebedkin, U. Schepers, M. M. Kappes, F. Biedermann and S. Bräse, *Small*, 2024, **20**, 2307318.
34 X. Qiu, T. Zheng, M. Runowski, P. Woźny, I. R. Martín, K. Soler-Carracedo, C. E. Piñero, S. Lebedkin, O. Fuhr and S. Bräse, *Adv. Funct. Mater.*, 2024, **34**, 2313517.
35 D. V. Berdnikova and E. Y. Chernikova, *ChemPhotoChem*, 2024, **8**, e202300140.
36 B. Yuan, H. Wu, H. Wang, B. Tang, J.-F. Xu and X. Zhang, *Angew. Chem., Int. Ed.*, 2021, **60**, 706–710.
37 J. Chen, S. Li, Z. Wang, Y. Pan, J. Wei, S. Lu, Q.-W. Zhang, L.-H. Wang and R. Wang, *Chem. Sci.*, 2021, **12**, 7727–7734.
38 H. Hu, H. Wang, Y. Yang, J.-F. Xu and X. Zhang, *Angew. Chem., Int. Ed.*, 2022, **61**, e202200799.
39 D. Wu, J. Wang, X. Du, Y. Cao, K. Ping and D. Liu, *J. Nanobiotechnol.*, 2024, **22**, 235.
40 Q. Li, P. Zhang, P. Wang, C. Yan, K. Wang, W. Yang, D. Dang and L. Cao, *Aggregate*, 2025, **6**, e676.
41 Z. Wang, Z. Yang, S. Li, C. H. T. Kwong, D. Zhang, J. Wei, C. Gao, Q.-w. Zhang and R. Wang, *Adv. Funct. Mater.*, 2025, **35**, 2411070.
42 H. Ma, W. Xu, X. Tang, Y. Kang, J.-F. Xu and X. Zhang, *CCS Chem.*, 2025, **7**, 832–842.
43 Y. Yuan, X. Tang, X.-Y. Du, Y. Hu, Y.-J. Yu, Z.-Q. Jiang, L.-S. Liao and S.-T. Lee, *Adv. Opt. Mater.*, 2019, **7**, 1801536.
44 S. Madayanad Suresh, D. Hall, D. Beljonne, Y. Olivier and E. Zysman-Colman, *Adv. Funct. Mater.*, 2020, **30**, 1908677.
45 D. Hall, S. M. Suresh, P. L. dos Santos, E. Duda, S. Bagnich, A. Pershin, P. Rajamalli, D. B. Cordes, A. M. Z. Slawin, D. Beljonne, A. Köhler, I. D. W. Samuel, Y. Olivier and E. Zysman-Colman, *Adv. Opt. Mater.*, 2020, **8**, 1901627.
46 H.-Z. Li, F.-M. Xie, Y.-Q. Li and J.-X. Tang, *J. Mater. Chem. C*, 2023, **11**, 6471–6511.
47 X. Wu, S. Ni, C.-H. Wang, W. Zhu and P.-T. Chou, *Chem. Rev.*, 2025, **125**, 6685–6752.
48 C. Si, W. L. Primrose, Y. Xu, Z. M. Hudson and E. Zysman-Colman, *Adv. Opt. Mater.*, 2025, **13**, 2402576.
49 P. Hu, W. L. Primrose and Z. M. Hudson, *Adv. Opt. Mater.*, 2025, **13**, 2403409.
50 S. J. Barrow, S. Kasera, M. J. Rowland, J. del Barrio and O. A. Scherman, *Chem. Rev.*, 2015, **115**, 12320–12406.
51 X. Qiu, J. Seibert, O. Fuhr, F. Biedermann and S. Bräse, *Chem. Commun.*, 2024, **60**, 3267–3270.
52 F. Liu, H. Xiao, Q. Gao, D. Siri, D. Bardelang, Q. Xing and J. Geng, *Chem. Commun.*, 2025, **61**, 6675–6678.
53 P. Thordarson, *Chem. Soc. Rev.*, 2011, **40**, 1305–1323.
54 S. Wu, W. Li, K. Yoshida, D. Hall, S. Madayanad Suresh, T. Sayner, J. Gong, D. Beljonne, Y. Olivier, I. D. W. Samuel and E. Zysman-Colman, *ACS Appl. Mater. Interfaces*, 2022, **14**, 22341–22352.

55 G. Chen, J. Wang, W.-C. Chen, Y. Gong, N. Zhuang, H. Liang, L. Xing, Y. Liu, S. Ji, H.-L. Zhang, Z. Zhao, Y. Huo and B. Z. Tang, *Adv. Funct. Mater.*, 2023, **33**, 2211893.
56 S. Diesing, L. Zhang, E. Zysman-Colman and I. D. W. Samuel, *Nature*, 2024, **627**, 747–753.
57 D. C. Neckers, *J. Photochem. Photobiol., A*, 1989, **47**, 1–29.
58 K. H. Jones and J. A. Senft, *J. Histochem. Cytochem.*, 1985, **33**, 77–79.